scientific reports

Check for updates

OPEN

# Dynamic load frequency control in Power systems using a hybrid simulated annealing based Quadratic Interpolation Optimizer

Davut Izci[1,2], Serdar Ekinci[1], Emre Çelik[3], Mohit Bajaj[4,5,6]✉, Vojtech Blazek[7] & Lukas Prokop[7]

**Ensuring the stability and reliability of modern power systems is increasingly challenging due to the growing integration of renewable energy sources and the dynamic nature of load demands. Traditional proportional-integral-derivative (PID) controllers, while widely used, often fall short in effectively managing these complexities. This paper introduces a novel approach to load frequency control (LFC) by proposing a filtered PID (PID-F) controller optimized through a hybrid simulated annealing based quadratic interpolation optimizer (hSA-QIO). The hSA-QIO uniquely combines the local search capabilities of simulated annealing (SA) with the global optimization strengths of the quadratic interpolation optimizer (QIO), providing a robust and efficient solution for LFC challenges. The key contributions of this study include the development and application of the hSA-QIO, which significantly enhances the performance of the PID-F controller. The proposed hSA-QIO was evaluated on unimodal, multimodal, and low-dimensional benchmark functions, to demonstrate its robustness and effectiveness across diverse optimization scenarios. The results showed significant improvements in solution quality compared to the original QIO, with lower objective function values and faster convergence. Applied to a two-area interconnected power system with hybrid photovoltaic-thermal power generation, the hSA-QIO-tuned controller achieved a substantial reduction in the integral of time-weighted absolute error by 23.4%, from 1.1396 to 0.87412. Additionally, the controller reduced the settling time for frequency deviations in Area 1 by 9.9%, from 1.0574 s to 0.96191 s, and decreased the overshoot by 8.8%. In Area 2, the settling time was improved to 0.89209 s, with a reduction in overshoot by 4.8%. The controller also demonstrated superior tie-line power regulation, achieving immediate response with minimal overshoot.**

**Keywords** Quadratic interpolation optimizer, Simulated annealing, Load frequency control, Filtered PID controller, Two-area photovoltaic-thermal power system, Power system stability

Load frequency control (LFC) is essential for maintaining power balance between interconnected areas under varying load conditions, playing a critical role in ensuring the stability of power systems. The presence of LFC is vital to the efficient operation and stability of these systems[1]. In contemporary power systems, grid stability and reliability are paramount, as they ensure a consistent and high-quality electricity supply. Among the numerous challenges faced by power systems, LFC is particularly significant, especially as modern power networks grow in size and complexity. The appeal of LFC is further heightened by the limitations of traditional units, such as high maintenance costs and environmental restrictions. Currently, addressing LFC is crucial to ensuring that consumers receive reliable, high-quality power, especially in scenarios where load demand fluctuates significantly, system structures change, and the size of power system units increases[2]. In this application, traditional proportional-integral-derivative (PID) controllers have been widely used[3–5]. However, these

[1]Department of Computer Engineering, Batman University, Batman 72100, Turkey. [2]Applied Science Research Center, Applied Science Private University, Amman 11931, Jordan. [3]Department of Electrical and Electronics Engineering, Düzce University, Düzce, Turkey. [4]Department of Electrical Engineering, Graphic Era (Deemed to be University), Dehradun 248002, India. [5]Department of Electrical Engineering, Graphic Era Hill University, Dehradun 248002, India. [6]College of Engineering, University of Business and Technology, Jeddah 21448, Saudi Arabia. [7]ENET Centre, VSB-Technical University of Ostrava, 708 00 Ostrava, Czech Republic. ✉email: thebestbajaj@gmail.com

conventional methods increasingly fall short in addressing the dynamic challenges presented by modern power systems.

In the last few decades, a number of control schemes have been proposed to effectively maintain the nominal values of tie-line interchange power and system frequency, even in the event of system failure. The LFC of a multi-area system with distributed producing resources, a gate-controlled series capacitor, and a high-voltage direct current connection was examined in the research[6,7]. As a supplementary controller, the researchers developed a proportional integral fractional derivative controller in Ref.[6], which they then optimized using the ant lion optimizer technique. The previously outlined tactics enhanced the power system's dynamic stability; however, their use necessitates substantial computer resources. Among other things, the controller's high order, complexity, requirement for a sizable training data set, defuzzification processes, and inference method made it unsuitable for real-time deployment. Numerous techniques, such as the genetic algorithm[8], particle swarm optimization[9], flower pollination algorithm[10], firefly algorithm[11], and hybrid improved gravitational search algorithm – binary particle search optimization[12], have been developed for optimizing PI, PID and fractional order PID (FOPID) controller settings.

Ekinci et al.[13] developed a novel hybrid educational competition optimizer combined with a pattern search and cascaded PDN-PI controller to regulate the frequency of PV-reheat thermal power systems, showcasing the potential of hybrid optimization in maintaining stability in renewable-integrated grids. Building on this, Jabari et al.[14] focused on the efficiency of a multi-stage FOPD(1 + PI) controller optimized by the Pelican optimization algorithm for DC motor speed control, further emphasizing the role of optimization algorithms in dynamic control systems. Similarly, Pachauri et al.[15] proposed a robust fractional-order control scheme for PV-penetrated microgrids, illustrating the growing complexity of control in grids with high renewable integration. This need for advanced control is echoed in Kalyan et al.[16], who applied the Squirrel Search Algorithm for interconnected power systems, highlighting the adaptability of nature-inspired algorithms in load frequency control (LFC). Jena et al.[17] further emphasized the importance of energy storage, investigating the impact of redox flow batteries on the frequency stability of multi-area systems, which aligns with Begum et al.'s[18] work on intelligent fuzzy logic-based sliding mode controllers for stability in deregulated power systems. The focus on optimal control strategies is extended by Kalyan et al.[19], who assessed open-loop and closed-loop models for LFC in three-area reheat thermal systems, and subsequently explored fractional-order fuzzy controllers optimized by the Seagull Optimization Algorithm for managing diverse sources with constraints[20]. Their research connects to their previous work[21], where they used a water-cycle algorithm to tune intelligent fuzzy controllers, demonstrating the adaptability of such algorithms in complex, time-delay-prone systems. Kalyan et al.[22] also conducted a comparative performance assessment of energy storage devices, underscoring their critical role in maintaining system stability. Further emphasizing the need for intelligent control, Kalyan et al.[23] optimized a type-II fuzzy controller for multi-area multi-fuel systems with communication delays using the water-cycle algorithm. Their subsequent strategy[24], combining SMES and TCSC for multi-source systems using a 3DOF-PID controller, integrates energy storage and reactive power compensation for enhanced stability. This body of work culminates in their latest research[25,26], where they employed soft computing and hybrid fuzzy PID controllers for network stability and simultaneous voltage and frequency stabilization, underscoring the convergence of optimization techniques, intelligent control, and storage technologies in addressing modern power system challenges.

In the face of external disturbances and uncertainty in parameter values, the controller settings as initially designed may fail to deliver adequate performance. To address this, various population-based optimization techniques have been proposed to enhance the stability and robustness of systems[27]. Most of these tactics are specific, concentrating on particular problems or working best in particular scenarios. In specific situations, the current optimization techniques usually yield exceptional outcomes. It has been shown that utilizing the quasi-oppositional backtracking search algorithm is an efficacious strategy for managing the LFC in large-scale power systems[28]. This method has been utilized to address the LFC challenge in power systems. It involves designing optimal PID controllers for two different power systems, generated via computer simulation, and optimized using a fitness function based on integral time-weighted absolute error. The simulation results revealed that this technique outperformed other approaches, such as adaptive neuro-fuzzy inference systems, fuzzy logic, and artificial neural networks[29,30]. Its utility was illustrated by examining the constructed controller's response to different degrees of uncertainty. Even while these tactics work well, there are obstacles to overcome when using them in new situations. For instance, many algorithms might work great in steady-state conditions, but they might not handle sudden variations in load or generation well[27].

These constraints are crucial because real-time decision-making is critical in modern power systems. As a result, we require optimization techniques that are not only robust but also adaptable to the dynamic characteristics of contemporary power systems. Hybrid optimization methods have recently gained attention as a promising solution to these challenges. By integrating the strengths of multiple optimization approaches, these algorithms aim to surpass the limitations associated with using a single technique[31–36]. In our quest for an LFC strategy that is both highly efficient and globally adaptable, we have turned to hybrid optimization techniques. These hybrid algorithms leverage the best aspects of the combined methods, providing a comprehensive solution to LFC challenges.

Numerous studies have proposed a hybrid optimization approach for long-term care. By combining numerous algorithms, such as the firefly algorithm, learning-based optimization, particle swarm optimization, artificial bee colony, grey wolf optimization, and the shuffling frog leaping algorithm, this approach enhanced the performance of the LFC system[37–40]. To get the best LFC, these techniques were applied to modify the controller settings in multi-area power systems. The simulation results show that hybrid optimization procedures are more successful and superior regarding rising time, settling time, and steady-state frequency deviation.

In light of this debate, hybrid optimization[41–43] in the context of LFC is still a developing subject, necessitating further study to evaluate the efficacy and utility of these methods. In this context, the study question is whether

any other effective optimization techniques have yet been utilized in the field of LFC. The goal of this research is to create an algorithm called hybrid simulated annealing (SA)[44] based quadratic interpolation optimizer (QIO)[45] to handle LFC in a two-area interconnected power system.

The QIO utilizes the mathematical concept of minimizing quadratic functions to achieve effective global search capabilities. On the other hand, the SA algorithm enhances local search by simulating the annealing process in metallurgy and relying on stochastic and single solution-based methods. The combination of these two algorithms (hSA-QIO) creates a unique and powerful tuning mechanism for LFC, resulting in improved performance and resilience. The hybrid method incorporates the SA as an integral component of the QIO, rather than executing both algorithms sequentially. That enables SA to explore suboptimal alternatives in order to avoid disregarding the potential of neighboring options. To validate the robustness and general applicability of the proposed hSA-QIO, its performance was evaluated on a set of benchmark functions, including unimodal, multimodal, and low-dimensional test cases. This comprehensive analysis provided insights into the algorithm's capability to handle various optimization challenges beyond the load frequency control context.

In the LFC application, the proposed hSA-QIO method was utilized to optimize the parameters of a filtered PID (PID-F) controller[46]. The motivation for using a PID-F controller was its capacity to increase the performance and resilience of a traditional PID controller by including a filter, especially in the presence of high-frequency noise[47]. Statistical analysis, convergence behavior, robustness analysis with regard to the well-known integral of error-based performance indicators[43], the effect of solar radiation fluctuation in photovoltaic unit, and random load variation on thermal unit were all evaluated. The statistical study clearly shown that the suggested hSA-QIO outperforms the other methods in optimizing the PID-F controller for the hybrid photovoltaic-thermal power system. hSA-QIO's improved performance and stability make it an extremely effective solution for tackling this context's load frequency control problem. The convergence profile study demonstrated the hSA-QIO algorithm's benefits in terms of faster convergence and better reduction of the integral of the time-weighted absolute error objective function. This makes hSA-QIO a more efficient and dependable option for improving the PID-F controller in a hybrid photovoltaic-thermal power system. The hSA-QIO-based PID-F controller outperformed the other techniques in terms of shorter settling times, decreased overshoot, and reduced undershoot. This makes it the best option for improving the PID-F controller in a hybrid photovoltaic-thermal power system, resulting in robust and efficient load frequency regulation. Furthermore, the hSA-QIO-based PID-F controller exhibits the best behavior across all performance indices (integral of absolute error, integral of squared error, and integral of time-weighted squared error), demonstrating its resilience and efficacy. The suggested strategy effectively reduces both the amplitude and persistence of errors, resulting in faster stabilization and better performance than prior methods.

The findings show that the hSA-QIO-based PID-F controller is extremely successful in managing and controlling system deviations, delivering consistent and steady performance in two-area power system operations. Despite changes in photovoltaic power output, the hSA-QIO-tuned PID-F controller successfully regulates frequency variations and tie-line power. Despite variations in load, the hSA-QIO-tuned PID-F controller retains its transient responsiveness. This demonstrates the controller's durability and flexibility to load changes, which ensures the power supply remains stable. In summary, this work offers several noteworthy contributions to advancing the area of power system control:

- A novel hybrid metaheuristic algorithm, hSA-QIO, is introduced for tuning LFC controllers.
- The SA is embedded as part of the QIO in order to avoid computational burden.
- The statistical performance of the hSA-QIO is shown through various benchmark functions.
- PID-F controller is presented to mitigate disturbances effectively.
- Enhanced performance and robustness of the hSA-QIO-tuned PID-F controller is demonstrated for a two-area photovoltaic-thermal power system.
- Comprehensive comparison with existing control methods showcases the superiority of the proposed approach.

## The proposed methodology

### Basics of quadratic interpolation optimizer

The QIO algorithm is a powerful optimization technique designed to efficiently locate the minimum of a given function by leveraging quadratic interpolation[45]. The core idea behind QIO is to construct a quadratic model based on a set of sampled points from the search space, which can then be used to predict the location of the function's minimum. This prediction guides the optimization process, making it both precise and effective, particularly for problems with a smooth underlying structure.

The generalized quadratic interpolation (GQI) method forms the central component of QIO[45]. This method involves constructing a quadratic function that passes through three selected points in the search space: the current solution $x_i$, and two additional points, $x_{j1}$ and $x_{j2}$, which are chosen based on the algorithm's specific strategy (e.g., randomly or based on fitness). The quadratic function can be expressed as:

$$f(x) = ax^2 + bx + c \tag{1}$$

where $a$, $b$, and $c$ are coefficients determined by solving the system of equations formed by substituting the three points into the quadratic function:

$$\begin{cases} f(x_i) = a{x_i}^2 + bx_i + c \\ f(x_{j1}) = a{x_{j1}}^2 + bx_{j1} + c \\ f(x_{j2}) = a{x_{j2}}^2 + bx_{j2} + c \end{cases} \tag{2}$$

Solving this system yields the coefficients $a$, $b$, and $c$, thereby fully defining the quadratic model. The next step in QIO is to find the minimizer of the quadratic function, which represents the predicted location of the function's minimum. The minimizer can be calculated analytically as:

$$x_{min} = -\frac{b}{2a} \tag{3}$$

This minimizer $x_{min}$ is then used to update the current solution, guiding the algorithm closer to the global minimum[45]. In light of the above presentation, the steps of the QIO can be expressed as follows:

i. The algorithm begins by initializing a population of $N$ individuals (candidate solutions) in the search space. Each individual $x_i$ is randomly positioned within the feasible solution space for the optimization problem. The fitness function $f(x_i)$ is then calculated for each individual in the population. The best individual, $x_{best}$, and its corresponding fitness $f(x_{best})$ are recorded. The general objective is to minimize (or maximize) $f(x_i)$ depending on the problem formulation.

ii. In the exploration phase, the QIO algorithm aims to explore new regions in the search space to avoid premature convergence. For each dimension $j$ of an individual $x_i$, two other individuals, $x_k$ and $x_l$, are randomly selected from the population. A GQI method is then used to compute the minimizer $x_j^*$ of the quadratic interpolation function formed by the positions $x_i$, $x_k$, and $x_l$. This helps maintain population diversity and expands the search to potentially unexplored regions. The new position is updated based on the calculated minimizer and an additional exploration term. Mathematically, the update equation for the exploration phase is:

$$v_i(t+1) = x^*_{i,rand1,rand2}(t) + w_1 \cdot \left(x_{rand3}(t) - x^*_{i,rand1,rand2}(t)\right) + round(0.5 \cdot (0.05 + r1)) \cdot log\left(\frac{r2}{r3}\right) \tag{4}$$

$$x^*_{i,rand1,rand2}(t) = GQI(x_i(t),\ x_{rand1}(t), x_{rand2}(t),\ f(x_i(t)),\ f(x_{rand1}(t)),\ f(x_{rand2}(t))) \tag{5}$$

where $x^*_{i,rand1,rand2}(t)$ is the minimizer derived from the GQI method for the current individual and two randomly selected individuals, and $w_1$, $r1$, $r2$, and $r3$ are control parameters to balance exploration and exploitation.

iii. During exploitation, the algorithm focuses on refining the current best solutions. For each dimension $j$, the minimizer $x_j^*$ of the quadratic interpolation function formed by the current individual $x_i$, the best solution so far $x_{best}$, and another random individual is calculated using the GQI method. The updated position is generated by incorporating this minimizer. The minimizer of the quadratic interpolation function formed by these three individuals is computed, and the position of the current individual is updated accordingly. The exploitation strategy ensures that local searches are more targeted and efficient by focusing on the refinement of solutions around the best-known regions. The updated position in the exploitation phase is computed using:

$$v_i(t+1) = x^*_{beat,rand1,rand2}(t) + w_2 \cdot (x_{best}(t) - round(1 + rand) \cdot \left(\frac{Ub - Lb}{Ub^{rD} - Lb^{rD}}\right) \cdot x_i^{rD}(t) \tag{6}$$

$$x^*_{best,\,rand1,rand2}(t) = GQI(x_{best}(t),\ x_{rand1}(t), x_{rand2}(t),\ f(x_{best}(t)),\ f(x_{rand1}(t)),\ f(x_{rand2}(t))) \tag{7}$$

where $x^*_{best,\,rand1,rand2}(t)$ is the minimizer derived from the GQI method using the current individual, the best individual, and a randomly selected one. The factor $w_2$ controls the step size, ensuring a balance between local exploitation and broader searches.

iv. After performing exploration and exploitation, the position of each individual is updated based on the calculated minimizers. In this regard, the following expression is used.

$$x_i(t+1) = \begin{cases} x_i(t); f(x_i(t)) \leq f(v_i(t+1)) \\ v_i(t+1); f(x_i(t)) > f(v_i(t+1)) \end{cases} \tag{8}$$

v. The above process is repeated iteratively until a stopping criterion (e.g., maximum number of iterations or convergence) is met.

### Simulated annealing technique

The SA technique emulates the annealing process in metallurgy and is categorized as a single solution approach[48]. The method involves a series of heating and cooling steps, which ultimately results in the production of homogeneous crystals with fewer flaws. The SA begins by assigning a random value to the first solution, $x_i$, and then proceeds to generate a neighboring solution, $x_i'$, based on this initial value. Then, it calculates the fitness value for both $x_i$ and $x_i'$. If the fitness value of $x_i'$ ($f(x_i')$) is lower than that of $x_i$ ($f(x_i)$), then SA assigns $x_i = x_i'$. Meanwhile, SA may substitute the solution of $x_i$ with the solution of $x_i'$ even if the fitness values do not exhibit the same connection. The solution for this situation is determined by the probability $p$, which is specified as:

$$p = e^{-\frac{\Delta f}{T_k}} \; ; \; \Delta f = f(x_i') - f(x_i) \tag{9}$$

Here, $f$ and $T$ represent the control parameters of the fitness function and temperature, respectively. If the value of $p$ is less than a randomly generated number between 0 and 1, the method will not substitute $x_i$ with $x_i'$. However, if $p$ is more than or equal to the randomly generated number, a replacement will occur. The simulated annealing technique subsequently decreases the temperature value using the following equation, where $\mu$ represents the cooling coefficient which is a random constant ranging from 0 to 1.

$$T_{k+1} = \mu \, T_k \tag{10}$$

### The hybrid hSA-QIO approach

The proposed hSA-QIO approach is a hybrid integration of the QIO and SA algorithms. The necessity of the proposed hybrid hSA-QIO stems from the complementary strengths of the two optimization techniques involved. The original QIO is particularly effective for high-dimensional optimization problems and has shown promising results in various engineering applications. It is designed to be highly adaptable and can be integrated with other optimization algorithms to enhance their performance[45]. Similarly, SA is a metaheuristic algorithm that is widely employed to tackle both continuous and discrete optimization problems[48]. While QIO is highly effective in exploiting the local search space through its interpolation mechanism, it can be prone to premature convergence, especially in complex and multimodal landscapes. On the other hand, SA excels in exploration by enabling the algorithm to escape local optima, thanks to its probabilistic acceptance of suboptimal solutions. One key advantage of SA is its ability to overcome local minima through hill-climbing mechanisms, which is valuable for finding global solutions. To capitalize on this, a hybrid strategy is introduced in this work by incorporating SA to aid QIO in bypassing local minima and enhancing diversity during the search for an optimal solution. Integrating SA within the QIO framework thus provides a powerful means of refining the optimization process. The innovative hybrid method, hSA-QIO, effectively combines the capability of QIO with the hill-climbing attribute of SA in order to address the LFC design challenge.

Figure 1 presents a flowchart of the proposed hSA-QIO method. The flowchart illustrates that the process starts with configuring the control parameters and initializing the population of candidate solutions. The algorithm then enters a loop, where it first evaluates the fitness of the population. If the stopping condition (maximum number of iterations) is not met, the algorithm checks if any individual's fitness is better than the current best and updates the best solution accordingly. Then, the SA mechanism generates a new solution within the neighborhood of the current solution and calculates the change in fitness. The acceptance of this new solution is determined based on the SA acceptance probability, balancing between exploration and the likelihood of accepting worse solutions for broader search space coverage. For further refinement, the algorithm applies the QIO strategy. It randomly selects two individuals from the population and applies the generalized quadratic interpolation method to either perform exploration by considering the current solution or exploitation by incorporating the best solution found so far. Each individual in the population is updated based on these operations. Finally, the algorithm updates the temperature according to the cooling schedule, reducing it for the next iteration. This process repeats until the stopping condition (maximum number of iterations) is met, ensuring a balanced exploration-exploitation approach to finding the global optimum.

## Performance evaluation on benchmark functions

To assess the effectiveness and robustness of the proposed hSA-QIO algorithm, we tested its performance on various benchmark functions, categorized as unimodal, multimodal, and low-dimensional functions. The key functions include:

- Rosenbrock function (unimodal): This function is known for its narrow valleys and slow convergence, making it challenging for optimization algorithms.
- Penalized function (multimodal): Characterized by numerous local minima, this function tests the global search capabilities of the algorithm.
- Hartman 6 function (low-dimensional): This function, with fewer dimensions, tests the algorithm's performance in identifying global optima in small search spaces.

The details regarding the dimension, boundaries and the optimum values are provided in Table 1. We performed 30 independent runs for each function, with a population size of 30 and a maximum of 500 iterations for each

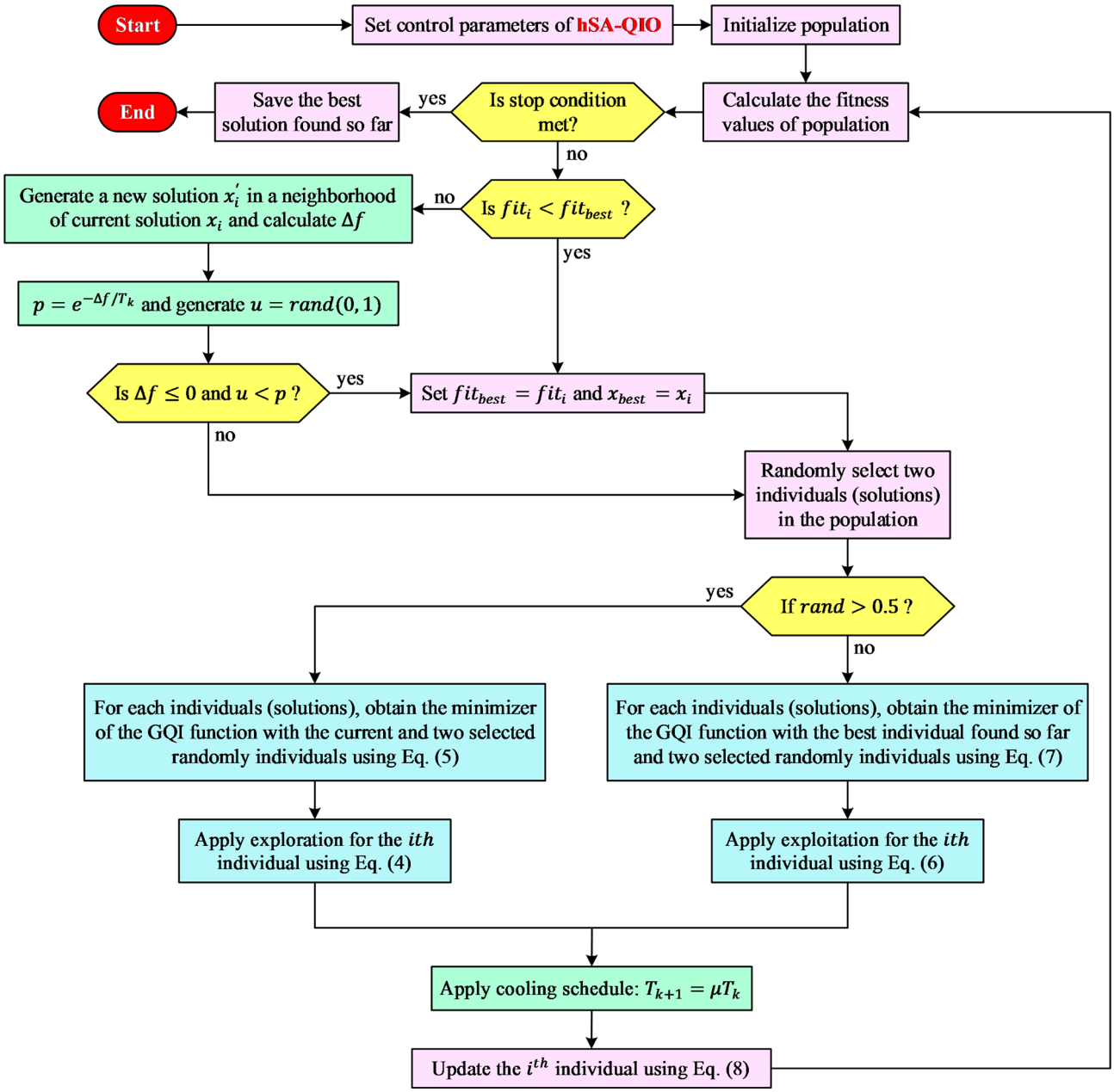


**Fig. 1**. Flowchart of proposed hSA-QIO method.

| Function name | Type | Dimension | Lower bound | Upper bound | Optimum |
|---|---|---|---|---|---|
| Rosenbrock | Unimodal | 30 | − 30 | 30 | 0 |
| Penalized | Multimodal | 30 | − 50 | 50 | 0 |
| Hartman 6 | Low-dimensional | 6 | 0 | 1 | − 3.322 |

**Table 1**. Details of used different benchmark functions.

run. The results were statistically analyzed, and the Wilcoxon signed-rank test was conducted to verify the significance of the results.

Table 2 provides the detailed statistical results for the hSA-QIO and original QIO algorithms. Metrics such as the best, mean, median, worst, and standard deviation values for each benchmark function are presented. The performance of the hSA-QIO is superior across all metrics, with significant improvements in solution quality, as evidenced by the Wilcoxon test p-values. The Rosenbrock function results show that the hSA-QIO achieves a significantly lower best value (7.0417E−12) compared to QIO (2.9839E−07), with a very small

| Function | Metric | hSA-QIO | QIO |
|---|---|---|---|
| Rosenbrock | Best | 7.0417E−12 | 2.9839E−07 |
| | Mean | 1.5172E−11 | 6.1175E−07 |
| | Median | 1.5329E−11 | 5.8884E−07 |
| | Worst | 2.1359E−11 | 8.6697E−07 |
| | Standard deviation | 3.5163E−12 | 1.2814E−07 |
| | p-value/Winner | 1.7344E−06 (hSA-QIO) | |
| | Average elapsed time (s) | 0.5620 | 0.5489 |
| Penalized | Best | 7.0912E−11 | 8.8552E−10 |
| | Mean | 1.1457E−10 | 3.8738E−09 |
| | Median | 1.1166E−10 | 3.9943E−09 |
| | Worst | 2.0774E−10 | 7.1875E−09 |
| | Standard deviation | 2.8711E−11 | 1.3472E−09 |
| | p-value/Winner | 1.7344E−06 (hSA-QIO) | |
| | Average elapsed time (s) | 0.5601 | 0.5423 |
| Hartman 6 | Best | −3.3220E+00 | −3.3220E+00 |
| | Mean | −3.3220E+00 | −3.2824E+00 |
| | Median | −3.3220E+00 | −3.3220E+00 |
| | Worst | −3.3220E+00 | −3.2031E+00 |
| | Standard deviation | 9.9893E−10 | 5.7008E−02 |
| | p-value/Winner | 1.9531E−03 (hSA-QIO) | |
| | Average elapsed time (s) | 0.5349 | 0.5246 |

**Table 2**. Statistical results and nonparametric Wilcoxon's test.

p-value of 1.7344E−06. This indicates that the proposed hSA-QIO significantly improves the solution quality while maintaining low variance, as evidenced by the lower standard deviation. In the penalized function, the hSA-QIO outperforms the QIO across all metrics. The best solution achieved by the hSA-QIO (7.0912E−11) is considerably better than that of the QIO (8.8552E−10), with a p-value of 1.7344E−06, confirming the statistical significance of this improvement. For the Hartman 6 function, both algorithms achieved the global minimum. However, the hSA-QIO had a tighter distribution with a smaller standard deviation (9.9893E−10), indicating that it consistently found the optimal solution with less variability across runs.

The computational time for each benchmark function was also analyzed. The average elapsed time for the hSA-QIO and QIO is also presented in Table 2. Although the hSA-QIO incurs a marginal increase in computational time (e.g., 0.5620 s for Rosenbrock compared to 0.5489 s for QIO), the improvement in solution quality justifies this negligible increase. The additional time is attributed to the integration of SA, which enhances the exploration-exploitation capabilities of the algorithm.

## Structure of PID with filter (PID-F) controller

The PID-F controller enhances the conventional PID controller by incorporating a filter to improve its performance and robustness[49], particularly in the presence of high-frequency noise[47]. This controller distinguishes itself from conventional PID and PI controllers by integrating a filter into the derivative term, significantly reducing the impact of high-frequency noise on the control signal. This feature enhances the stability and robustness of the system, especially in applications where noise and abrupt changes are common. As a result, the PID-F controller provides superior dynamic performance, better stability, and more precise control compared to classical PID and PI controllers, making it particularly suitable for high-speed industrial applications and systems with challenging operating conditions. The transfer function of the PID-F controller is given by[46]:

$$C_{PID-F}(s) = K_P + \frac{K_I}{s} + \frac{K_D N s}{s + N} \tag{11}$$

where $K_P$ is the proportional gain, $K_I$ is the integral gain, $K_D$ is the derivative gain, $N$ is the filter coefficient. The inclusion of the filter term $K_D N s/(s + N)$ helps to attenuate the high-frequency components that typically affect the derivative term, thus enhancing the overall stability and performance of the controller.

The block diagram of the PID-F controller, as illustrated in Fig. 2, demonstrates the structural arrangement of its components. The proportional, integral, and filtered derivative terms are combined to provide the control signal. This configuration ensures that the controller responds effectively to the error signal while mitigating the adverse effects of noise and other disturbances.

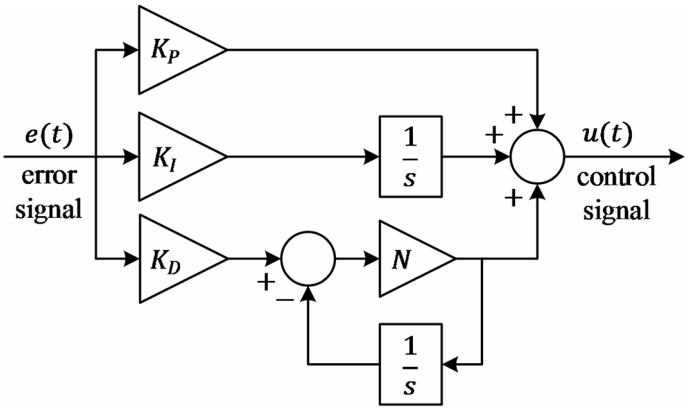


**Fig. 2**. Block diagram of PID-F controller.

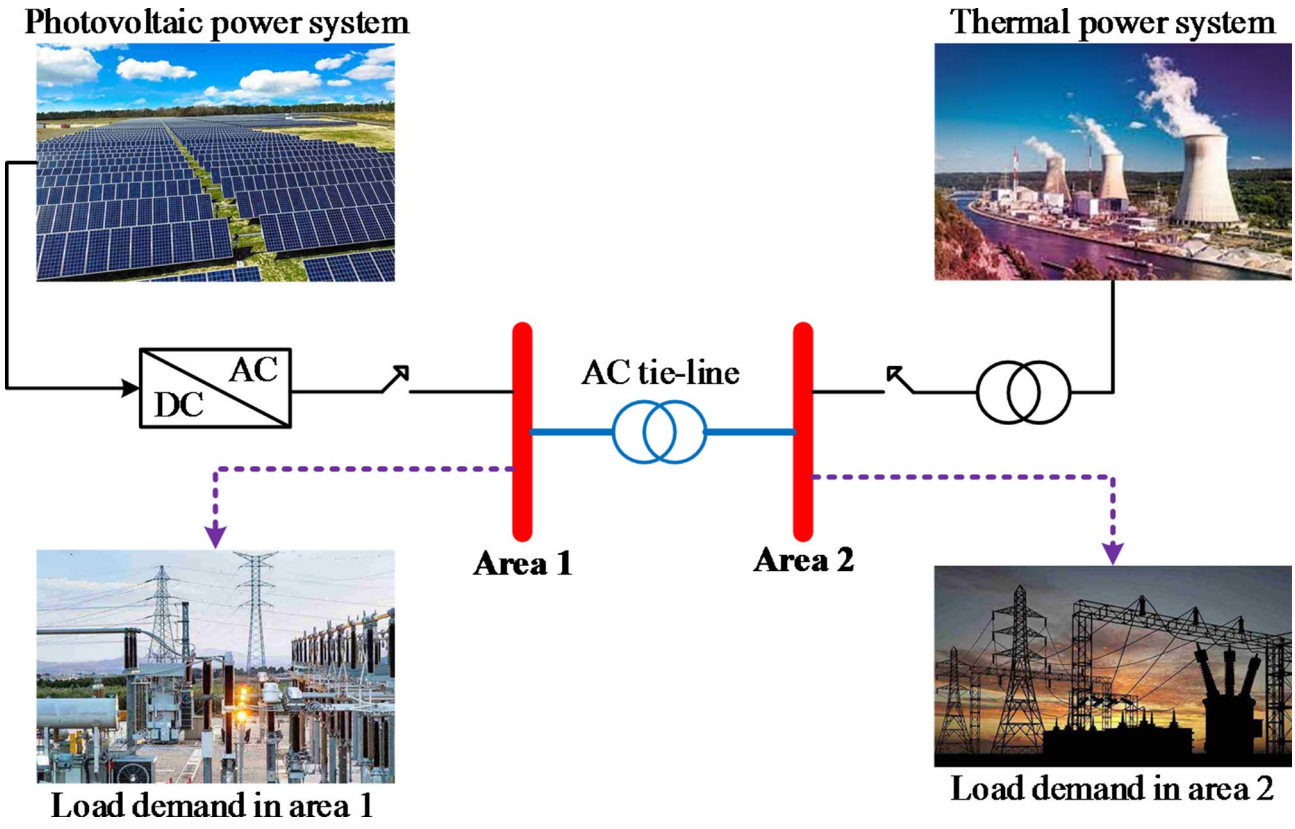


**Fig. 3**. Schematic diagram of power system.

## Modeling for hybrid PV-thermal power system

The hybrid PV-thermal power system integrates PV and thermal energy sources to enhance the efficiency and reliability of power generation[50]. The modeling of this system involves the transfer functions of its various components, each characterized by specific parameters. The schematic diagram of a hybrid PV-thermal power system is provided in Fig. 3 and the parameters and respective transfer functions of the components of this two-area system are provided in Table 3[51–54].

The PV system in area 1 is represented by a second-order transfer function, characterized by the parameters $M$, $N$, $C$, and $D$. Area 2 consists of a governor, turbine, reheater, and power system, each described by their respective first-order transfer functions and parameters. The governor's transfer function $G_{gov}(s)$ features a gain $K_g$ and a time constant $T_g$. The turbine is modeled by $G_{trb}(s)$ with parameters $K_t$ and $T_t$. The reheater is represented by $G_{rht}(s)$ with a gain $K_r$ and a time constant $T_r$. The overall power system transfer function $G_{ps}(s)$ includes a gain $K_p$ and a time constant $T_p$. Additional system parameters include the droop $R$, frequency bias $B$, and tie-line time constant $T_{12}$, which are critical for maintaining system stability and performance.

| Components | | Transfer function | Parameters and selected values |
|---|---|---|---|
| Area 1: PV system | | $G_{pv}(s) = \frac{-Ms+N}{s^2+Cs+D}$ | $M = 18,\ N = 900,\ C = 100$ and $D = 50$ |
| Area 2 | Governor | $G_{gov}(s) = \frac{K_g}{1+sT_g}$ | $K_g = 1$ and $T_g = 0.08$ s |
| | Turbine | $G_{trb}(s) = \frac{K_t}{1+sT_t}$ | $K_t = 1$ and $T_t = 0.3$ s |
| | Reheater | $G_{rht}(s) = \frac{sK_rT_r+1}{1+sT_r}$ | $K_r = 0.33$ and $T_r = 10$ s |
| | Power system | $G_{ps}(s) = \frac{K_p}{1+sT_p}$ | $K_p = 120$ and $T_p = 20$ s |
| Other parameters | | | $R = 2.5$ Hz/pu, $B = 0.8$ pu and $T_{12} = 0.545$ |

**Table 3**. Components, parameters and respective transfer functions of two-area system.

The detailed schematic diagram (Fig. 3) and parameters listed in Table 3 provide a comprehensive model for analyzing and optimizing the hybrid PV-thermal power system's dynamics and control strategies.

## Optimization problem

The optimization problem focuses on minimizing the integral of time-weighted absolute error (ITAE)[55] for the LFC problem in a hybrid PV-thermal power system. The ITAE is defined as:

$$ITAE = \int_0^{t_{sim}} t(|\Delta f_1| + |\Delta f_2| + |\Delta P_{tie}|)dt \tag{12}$$

where:

- $\Delta f_1$ and $\Delta f_2$ are the frequency deviations in area 1 and area 2, respectively.
- $\Delta P_{tie}$ is the tie-line power deviation.
- $t_{sim}$ is the simulation time, set to 30 s.

The ITAE objective function was selected for this study to ensure consistency with related works[51–54] that also use ITAE as their performance metric. This allows for a fair and reliable comparison of the proposed hSA-QIO algorithm with other approaches. Furthermore, ITAE is an ideal choice for load frequency control as it penalizes errors both in magnitude and over time, ensuring that the system achieves a stable and efficient response. The optimization process is conducted using the hSA-QIO with the following parameters:

- Population size: 50.
- Maximum number of iterations: 100.
- Number of independent runs: 20.

The tuning parameters for the PID-F controller are subject to the following constraints:

- $-2 \leq K_P \leq 2$
- $-2 \leq K_I \leq 2$
- $-2 \leq K_D \leq 2$
- $0.1 \leq N \leq 10$

The goal is to find the optimal values of $K_P$, $K_I$, $K_D$, and $N$ that minimize the ITAE, thereby ensuring efficient and stable control of the power system. The boundaries for the $K_P$, $K_I$, and $K_D$ gains of the PID-F controller were selected based on the ranges commonly used in similar studies in the literature[51–54]. These established boundaries provide a reliable starting point for optimization. The boundary for the filter coefficient ($N$) was determined through detailed analysis to ensure the controller's optimal performance in mitigating high-frequency noise and achieving robust system stability. The block diagram in Fig. 4 illustrates the design process of the PID-F controller using the hSA-QIO algorithm. This approach aims to enhance the LFC by optimizing the PID-F parameters, thereby improving the system's response to frequency and tie-line power deviations.

## Simulation results and discussion

### Statistical analysis

The simulation results provide a comprehensive evaluation of the performance of the proposed hSA-QIO in optimizing the PID-F controller for the hybrid PV-thermal power system. The statistical analysis is based on 20 independent runs, comparing the minimized ITAE values obtained using the hSA-QIO and QIO algorithms. Figure 5 provides a visual representation of the minimized ITAE values with respect to number of runs. On the other hand, Table 4 presents the detailed statistical results, including the best, mean, median, worst, and standard deviation values for both the original QIO and the proposed hSA-QIO.

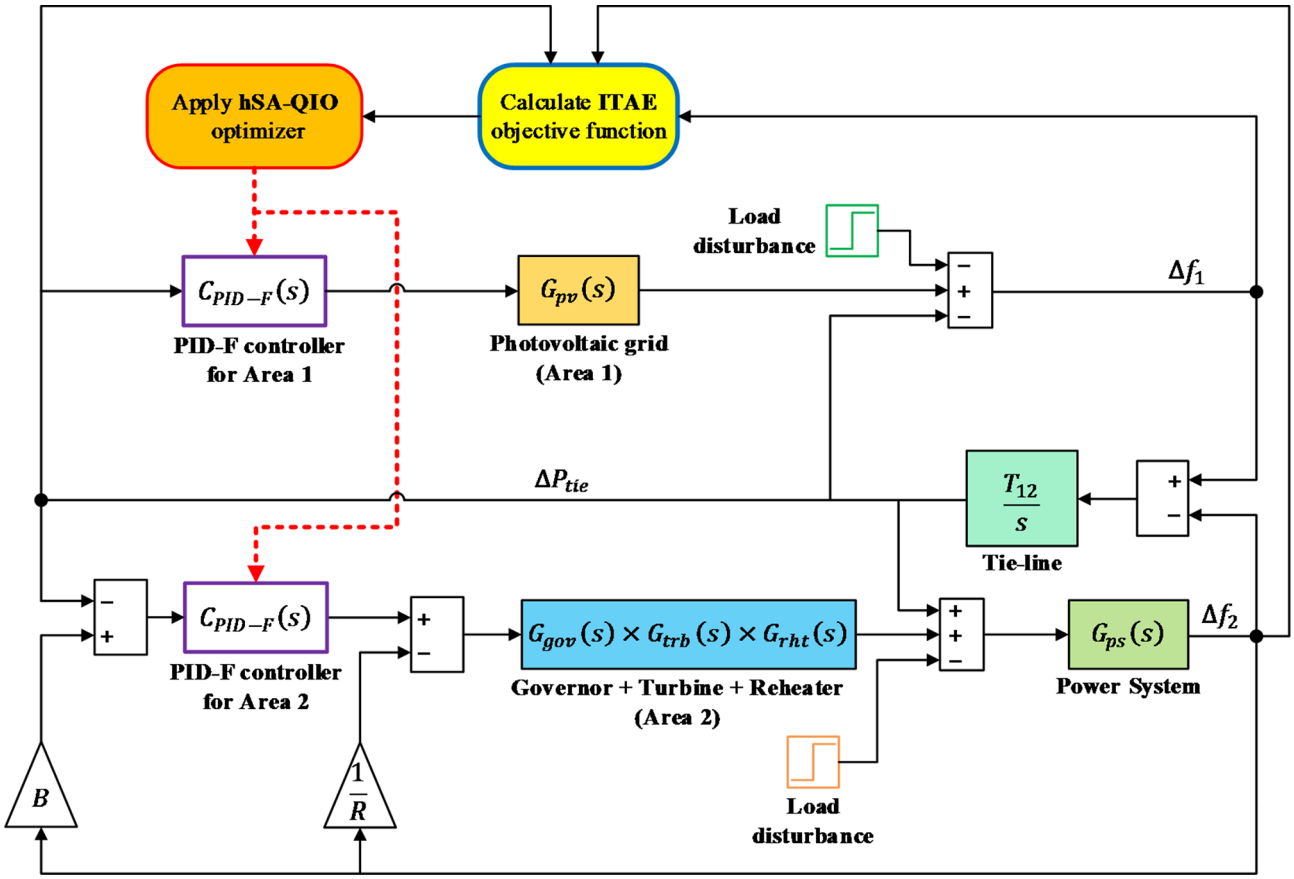


**Fig. 4**. Block diagram of hSA-QIO based PID-F controller design for LFC problem.

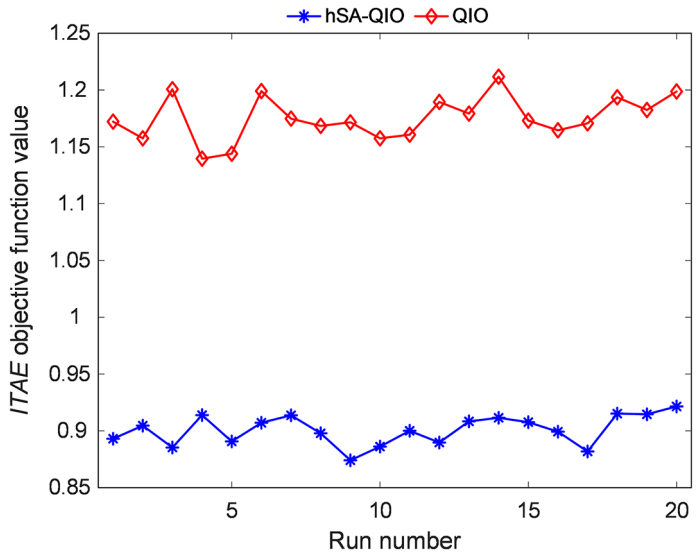


**Fig. 5**. The minimized ITAE values from independent 20 runs using hSA-QIO and QIO algorithms.

The results indicate that the hSA-QIO outperforms the original QIO algorithm across all metrics. Specifically, the hSA-QIO algorithm achieves a lower best ITAE value (0.87412) compared to the QIO (1.1396). Additionally, the mean, median, and worst ITAE values are consistently lower for the hSA-QIO, demonstrating its superior performance in minimizing the ITAE. The standard deviation of the ITAE values for the hSA-QIO (0.013086) is also smaller than that of the QIO (0.019207), indicating more consistent and reliable performance.

| Metric | hSA-QIO | QIO |
|---|---|---|
| Best | 0.87412 | 1.1396 |
| Mean | 0.90084 | 1.1755 |
| Median | 0.90235 | 1.1726 |
| Worst | 0.9215 | 1.2117 |
| Standard deviation | 0.013086 | 0.019207 |

**Table 4**. Statistical results obtained for original QIO and the proposed hSA-QIO.

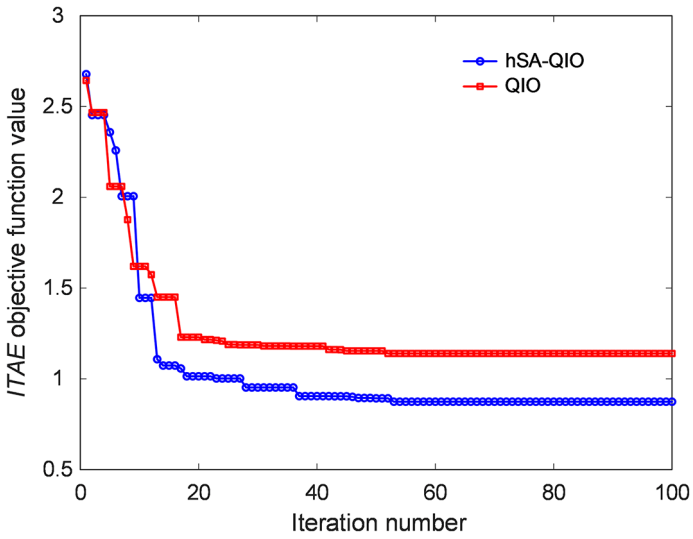


**Fig. 6**. Variation curves of ITAE objective function.

## Convergence profile of hSA-QIO and QIO algorithms

Figure 6 illustrates the convergence behavior of the QIO and hSA-QIO algorithms with respect to the ITAE objective function. As the number of iterations increases, both algorithms show a steady reduction in the ITAE values, converging to near-optimal solutions before reaching the maximum iteration limit (100). The hSA-QIO algorithm consistently outperforms the QIO algorithm by achieving lower ITAE values, demonstrating its superior solution quality and faster convergence. This highlights the enhanced performance of the hSA-QIO algorithm in optimizing the PID-F controller parameters for load frequency control.

## Performance comparison with recently reported studies

To evaluate the effectiveness of the hSA-QIO based PID-F controller, its performance is compared against several recently reported methods under a 0.1 p.u. load disruption (10% step change) in both areas of the two-area system. The compared methods include:

- Modified whale optimization algorithm (MWOA) based PID-F controller[51].
- Gorilla troops optimization (GTO) based PI controller[54].
- Salp swarm algorithm (SSA) based PI controller[53].
- Firefly algorithm (FA) based PI controller[52].

Table 5 demonstrates the controller parameters obtained via the reported approaches in the literature and the proposed approach in this study. These parameters are critical to assess the performance of the proposed approach with respect to the reported approaches. The time response specifications for frequency deviations in Area 1 ( $\Delta f_1$) and Area 2 ( $\Delta f_2$), as well as the tie-line power deviation ( $\Delta P_{tie}$), are critical metrics for assessing controller performance. The time response of the system is analyzed based on settling time, overshoot, and undershoot, with a $\pm$0.1 Hz tolerance band for $\Delta f_1$ and $\Delta f_2$, and a $\pm$0.025 MW tolerance band for $\Delta P_{tie}$ .

Figure 7 illustrates the time response of $\Delta f_1$ and the corresponding numerical values are presented in Table 6. The hSA-QIO based PID-F controller demonstrates the best performance for $\Delta f_1$, achieving the fastest settling time of 0.96191 s, which is significantly better than the other methods. It also has the lowest undershoot ($-$0.21764) and the smallest overshoot (0.0087999), indicating a more stable and accurate response to the load disruption.

Figure 8 illustrates the time response of $\Delta f_2$ and the corresponding numerical values are presented in Table 7. For $\Delta f_2$, the hSA-QIO based PID-F controller again shows superior performance with the second

| Controller type | Area 1 | | | | Area 2 | | | |
|---|---|---|---|---|---|---|---|---|
| | $K_P$ | $K_I$ | $K_D$ | $N$ | $K_P$ | $K_I$ | $K_D$ | $N$ |
| hSA-QIO based PID-F | −0.8713 | −0.1400 | −2 | 8.5934 | −2 | −2 | −0.2838 | 8.6406 |
| QIO based PID-F | −1.4915 | −0.1596 | −1.6127 | 4.1592 | −1.9998 | −2 | −0.1957 | 7.6569 |
| MWOA based PID-F | −1.9117 | −0.0649 | −1.5383 | 5.5236 | −1.8875 | −1.3179 | −0.1417 | 5.5236 |
| GTO based PI | −0.5235 | −0.0973 | – | – | −2 | −0.9238 | – | – |
| SSA based PI | −0.7715 | −0.0483 | – | – | −1.0837 | −0.8929 | – | – |
| FA based PI | −0.8811 | −0.5765 | – | – | −0.7626 | −0.8307 | – | – |

**Table 5**. Obtained controller parameters via different algorithms for area 1 and area 2.

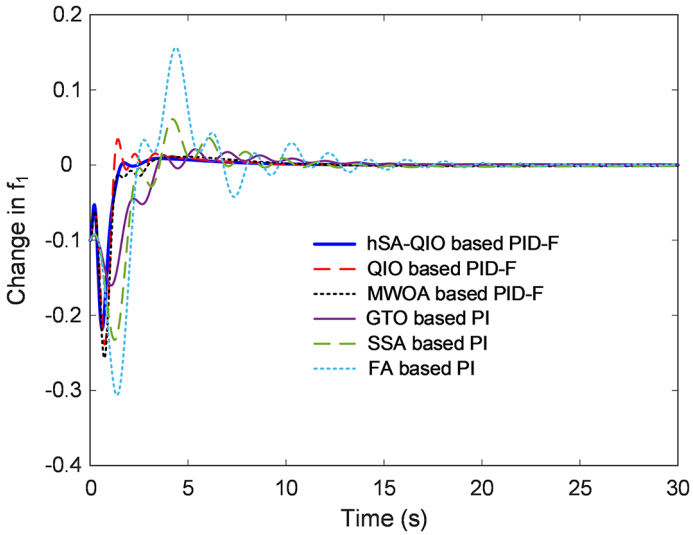


**Fig. 7**. Time response of $\Delta f_1$

| Controller type | Settling time (s) | Undershoot ($M^-$) | Overshoot ($M^+$) |
|---|---|---|---|
| hSA-QIO based PID-F | **0.96191** | **−0.21764** | **0.0087999** |
| QIO based PID-F | 1.0574 | −0.23868 | 0.034475 |
| MWOA based PID-F | 1.0827 | −0.25698 | 0.0111 |
| GTO based PI | 1.6234 | −0.16031 | 0.020943 |
| SSA based PI | 1.9059 | −0.23269 | 0.061061 |
| FA based PI | 4.8609 | −0.30629 | 0.15649 |

**Table 6**. Time response specifications for $\Delta f_1$. Significant values are given in bold.

fastest settling time of 0.89209 s. It also has the lowest undershoot (−0.18518) and the smallest overshoot (0.0081756), further proving its efficacy in maintaining system stability and accuracy.

Figure 9 illustrates the time response of $\Delta P_{tie}$ and the corresponding numerical values are presented in Table 8. The hSA-QIO based PID-F controller achieves a settling time of 0 s for $\Delta P_{tie}$, indicating an immediate response without any delay. It also has the lowest undershoot (−0.0055559) and minimal overshoot (0.0073026), highlighting its superior performance in managing tie-line power deviations.

## Robustness analysis via well-known integral of error-based performance indices

To thoroughly evaluate the robustness of the hSA-QIO based PID-F controller, apart from ITAE, we used several integral error-based performance indices, including the integral of absolute error (IAE), integral of squared error (ISE), and integral of time-weighted squared error (ITSE)[56]. These indices provide a comprehensive measure of the controller's performance over time, considering both magnitude and persistence of errors. The performance indices are defined as follows:

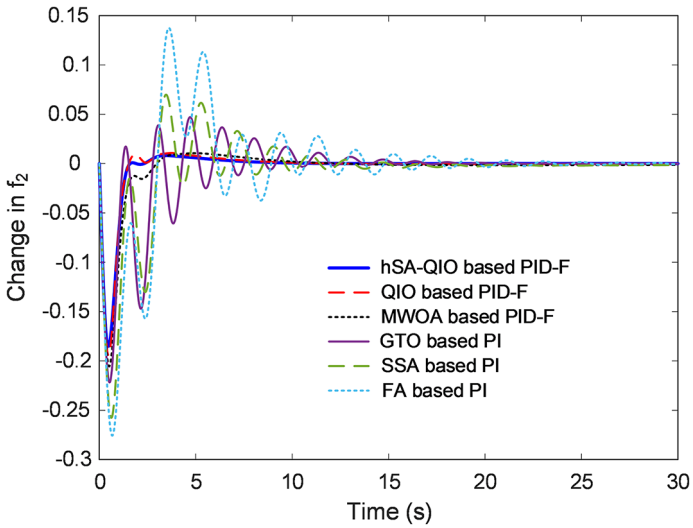


**Fig. 8**. Time response of $\Delta f_2$

| Controller type | Settling time (s) | Undershoot ($M^-$) | Overshoot ($M^+$) |
|---|---|---|---|
| hSA-QIO based PID-F | 0.89209 | **−0.18518** | **0.0081756** |
| QIO based PID-F | **0.88416** | −0.19458 | 0.010752 |
| MWOA based PID-F | 0.99792 | −0.20553 | 0.010527 |
| GTO based PI | 2.4497 | −0.22172 | 0.047077 |
| SSA based PI | 2.6428 | −0.25758 | 0.069851 |
| FA based PI | 5.6082 | −0.27569 | 0.13757 |

**Table 7**. Time response specifications for $\Delta f_2$. Significant values are given in bold.

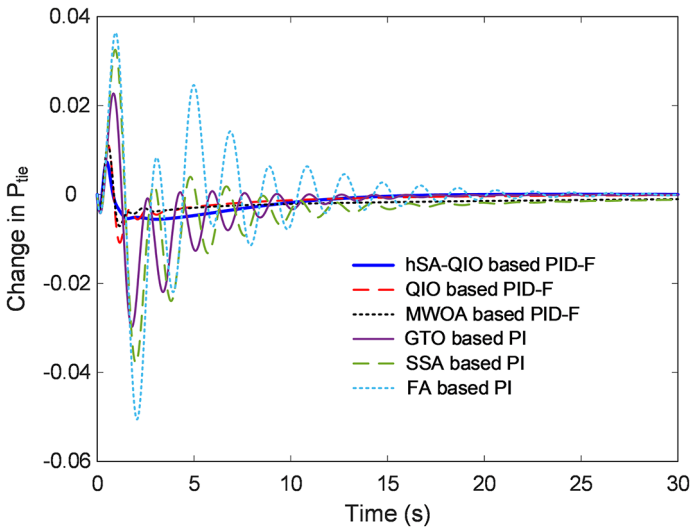


**Fig. 9**. Time response of $\Delta P_{tie}$

| Controller type | Settling time (s) | Undershoot ($M^-$) | Overshoot ($M^+$) |
|---|---|---|---|
| hSA-QIO based PID-F | **0** | **−0.0055559** | **0.0073026** |
| QIO based PID-F | **0** | −0.010806 | 0.011034 |
| MWOA based PID-F | 0 | −0.0070776 | 0.011044 |
| GTO based PI | 1.9898 | −0.029742 | 0.02272 |
| SSA based PI | 2.3188 | −0.037899 | 0.03253 |
| FA based PI | 2.5018 | −0.050536 | 0.036399 |

**Table 8**. Time response specifications for $\Delta P_{tie}$. Significant values are given in bold.

| Controller type | $IAE$ | $ITAE$ | $ISE$ | $ITSE$ |
|---|---|---|---|---|
| hSA-QIO based PID-F | **0.41625** | **0.87412** | **0.042149** | **0.026813** |
| QIO based PID-F | 0.46645 | 1.1396 | 0.04886 | 0.033762 |
| MWOA based PID-F | 0.59948 | 2.6198 | 0.059032 | 0.045505 |
| GTO based PI | 0.89859 | 2.9185 | 0.07738 | 0.10911 |
| SSA based PI | 1.1754 | 4.9948 | 0.12238 | 0.17743 |
| FA based PI | 1.7667 | 7.3783 | 0.22151 | 0.46346 |

**Table 9**. Obtained values for different performance metrics via different approaches. Significant values are given in bold.

$$IAE = \int_0^{t_{sim}} (|\Delta f_1| + |\Delta f_2| + |\Delta P_{tie}|)dt \tag{13}$$

$$ISE = \int_0^{t_{sim}} \left[(\Delta f_1)^2 + (\Delta f_2)^2 + (\Delta P_{tie})^2\right] dt \tag{14}$$

$$ITSE = \int_0^{t_{sim}} t\left[(\Delta f_1)^2 + (\Delta f_2)^2 + (\Delta P_{tie})^2\right] dt \tag{15}$$

The IAE measures the cumulative sum of the absolute error over the simulation period. It provides an indication of the total error magnitude without emphasizing the duration or severity of individual errors. Lower IAE values signify better overall control performance in minimizing deviations. The ISE metric squares the error before integration, which emphasizes larger errors more than smaller ones. It is particularly useful for highlighting the controller's ability to handle large deviations. The ITSE metric multiplies the squared error by time before integration, thus giving more weight to errors that occur later in the simulation. It helps evaluate the controller's performance in stabilizing the system over time.

Table 9 provides the values obtained for different performance metrics via different algorithms. The robustness analysis of the hSA-QIO based PID-F controller using well-known integral error-based performance indices—IAE, ITAE, ISE, and ITSE—demonstrates its superior performance compared to other methods. The hSA-QIO based PID-F controller achieves the lowest IAE (0.41625), indicating the best overall control in minimizing total error magnitude. It also excels in handling significant deviations with the lowest ISE (0.042149). Furthermore, the hSA-QIO controller shows outstanding long-term stability with the lowest ITSE (0.026813), reflecting efficient error correction over time. Compared to the QIO, MWOA, GTO, SSA, and FA based controllers, the hSA-QIO based PID-F controller consistently performs better across all indices, ensuring rapid stabilization and minimal persistent errors. These results confirm that the hSA-QIO based PID-F controller is highly effective in managing and controlling system deviations, providing reliable and stable performance in two-area power system operations.

## Influence of solar radiation variation in Area 1 on proposed controller

Simulations were performed to assess the influence of solar radiation fluctuation on the proposed controller during a time period ranging from 0 s to 80 s. Figure 10 depicts the changes in sun radiation at this period. The hSA-QIO-tuned PID-F controller's performance under these conditions was evaluated by analyzing its responses to frequency fluctuations and tie-line power deviation. Despite the fluctuations in PV power generation, the hSA-QIO-tuned PID-F controller effectively maintains the frequency variations and tie-line power at desired levels. Figure 11 depicts these reactions graphically, demonstrating the controller's capacity to govern the system under dynamic and unpredictable settings. This displays the controller's durability and responsiveness to variations in solar radiation, maintaining the power system's stability.

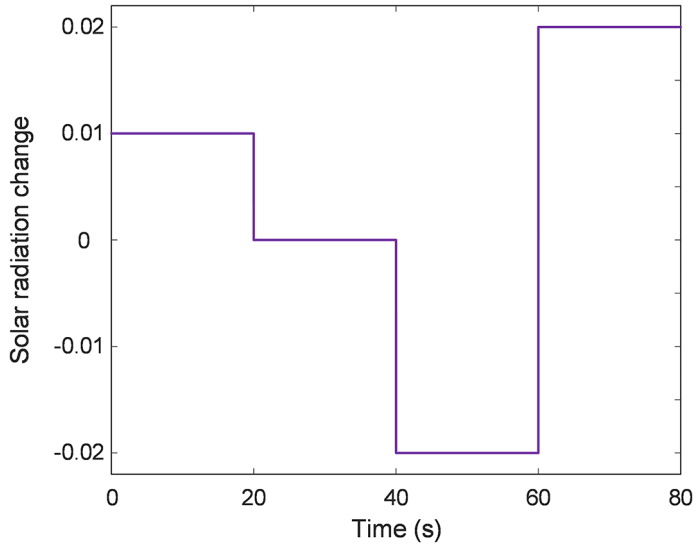


**Fig. 10**. Change of solar radiation.

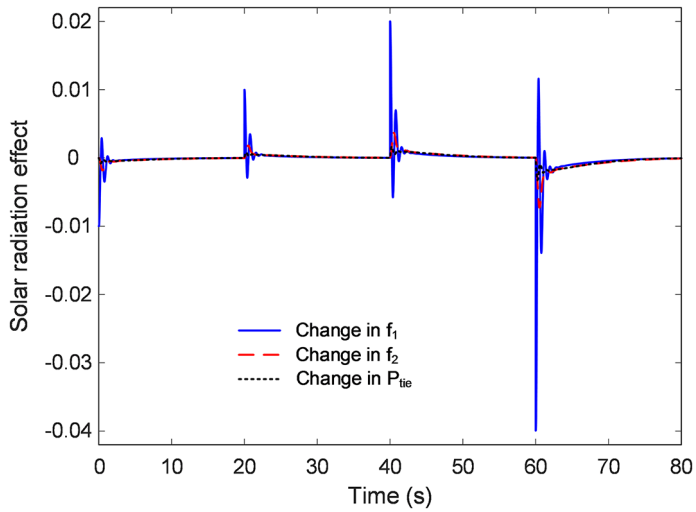


**Fig. 11**. Time response of hybrid PV-thermal power system.

## Influence of random load variation in area 2 on proposed controller

The influence of random load variation in area 2 was further investigated to provide better perspective on the performance of the proposed controller. Figure 12 shows the time response of $\Delta f_1$ to various load perturbations (0.1, 0.2, 0.3, and 0.4 pu), demonstrating the controller's capacity to govern the system under dynamic and unpredictable situations. Despite changes in load, the hSA-QIO-tuned PID-F controller maintains the time responsiveness of $\Delta f_1$. This displays the controller's durability and responsiveness to fluctuations in solar radiation, which ensures the power system's stability.

Figure 13 shows the time response for $\Delta f_2$ under similar load perturbations. The hSA-QIO-based PID-F method preserves the response for $\Delta f_2$, in the same manner as it does for $\Delta f_1$. Finally, Fig. 14 shows the time response for $\Delta P_{tie}$. It is obvious that the suggested technique is capable of maintaining time responsiveness for tie-line power in the presence of various load disturbances.

## Handling of power system non-linearity

The non-linear behavior of power systems, especially when integrating renewable energy sources such as photovoltaic units and dealing with load demand fluctuations, introduces complexities in system control. The proposed hSA-QIO algorithm is particularly suited for such environments due to its hybrid optimization approach. The QIO component efficiently models the system's response in near-linear regions, while the SA component allows the system to explore a broader solution space, overcoming local minima caused by non-linearities. In our experiments, we simulated several non-linear conditions, including variations in solar radiation

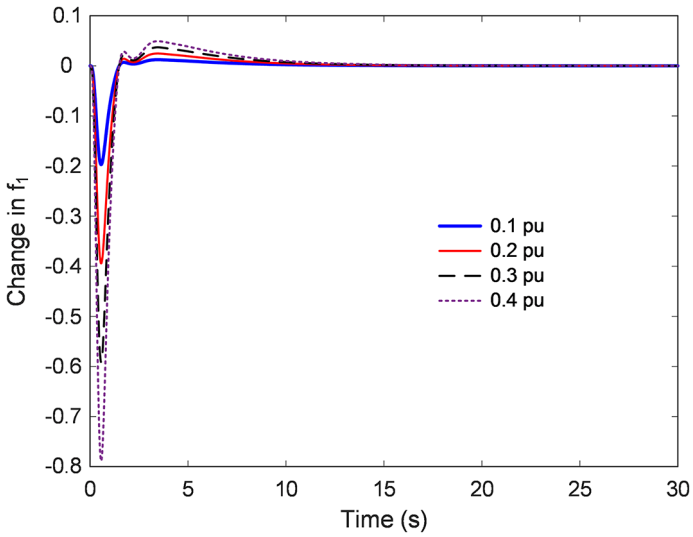


**Fig. 12**. Time response of $\Delta f_1$

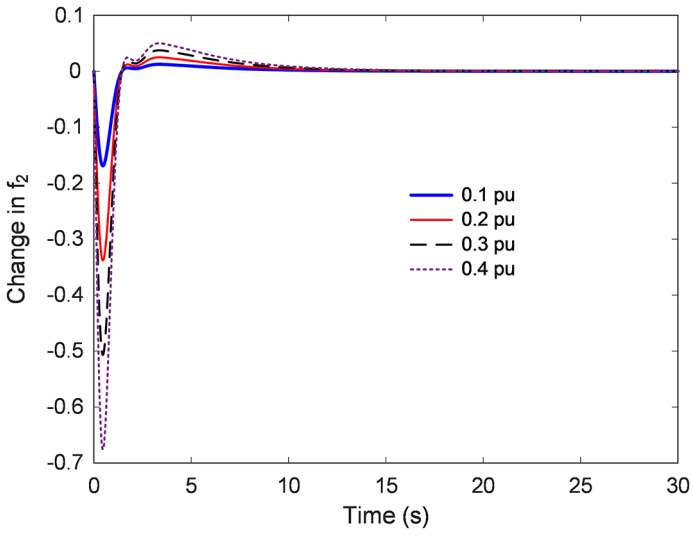


**Fig. 13**. Time response of $\Delta f_2$

and random load disturbances. The results showed that the hSA-QIO algorithm consistently outperformed other optimization techniques even in non-linear scenarios. This is because the probabilistic nature of simulated annealing allows the algorithm to escape local optima that are more likely to occur in non-linear regions of the solution space. By adjusting the step size dynamically, the algorithm remains robust across various non-linear conditions, ensuring efficient load frequency control under real-world complexities.

## Conclusion and future research directions

In present work, we introduced a novel hybrid hSA-QIO algorithm designed to address the challenges of LFC in modern power systems. The hSA-QIO effectively combines the strengths of SA and QIO, offering a powerful tool for optimizing the parameters of a PID-F controller in a two-area interconnected power system with hybrid photovoltaic-thermal power generation. The results of this research underscore the efficacy of the hSA-QIO algorithm in enhancing LFC performance. Specifically, the hSA-QIO-tuned PID-F controller achieved a notable reduction in the ITAE by 23.4%, alongside significant improvements in settling time and overshoot reduction in frequency deviations. The controller's ability to maintain tie-line power stability under varying load and generation conditions further highlights its robustness and reliability.

In addition to optimizing the LFC system, the proposed hSA-QIO was also tested on various benchmark functions to assess its performance across different optimization problems. The results demonstrated that hSA-QIO outperforms the original QIO in terms of convergence speed and solution quality, highlighting its potential applicability to a wider range of optimization tasks.

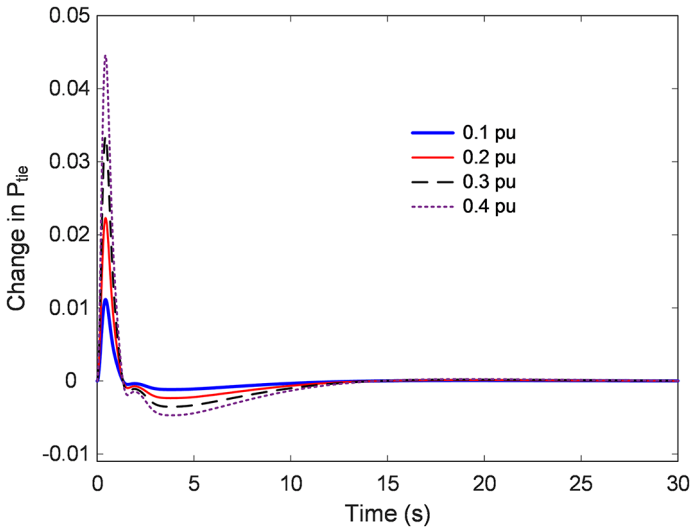


**Fig. 14**. Time response of $\Delta P_{tie}$

The promising results obtained from the application of the hSA-QIO in LFC open several avenues for future research. One significant direction involves expanding the application of hSA-QIO to multi-area and multi-source power systems, incorporating a broader range of renewable energy sources such as wind, biomass, and tidal power, to evaluate the algorithm's scalability and adaptability in more complex power system configurations. Additionally, implementing and testing the hSA-QIO in real-time control environments will provide valuable insights into its practical viability and effectiveness, particularly when integrated with real-time data acquisition and processing systems. Another promising research avenue is the integration of hSA-QIO with machine learning techniques to dynamically adjust optimization parameters based on system behavior predictions, thereby enhancing control strategies' efficiency and adaptability. Moreover, with the increasing risk of cyber-physical threats to power grids, future research could focus on enhancing the robustness of hSA-QIO-tuned controllers against such disruptions, ensuring the integrity of control systems in the face of cyber-physical attacks. Exploring other hybrid optimization techniques and comparing their performance with hSA-QIO could also lead to the discovery of even more effective methods, while applying hSA-QIO to other critical power system control problems, such as voltage stability, economic dispatch, and unit commitment, would further demonstrate its versatility. These future research directions aim to refine and extend the current work, addressing emerging challenges in power system control and contributing to the development of more stable, efficient, and secure power grids.

## Data availability

All data generated or analysed during this study are included in this published article.

Received: 20 August 2024; Accepted: 21 October 2024
Published online: 29 October 2024

## References

1. Iqbal, M. S. et al. A hybrid optimization algorithm for improving load frequency control in interconnected power systems. *Expert Syst. Appl.* **249**, 123702. https://doi.org/10.1016/j.eswa.2024.123702 (2024).
2. Subhasis Panda, S. et al. Residential demand side management model, optimization and future perspective: a review. *Energy Rep.* **8**, 3727–3766. https://doi.org/10.1016/j.egyr.2022.02.300 (2022).
3. Izci, D., Ekinci, S. & Hussien, A. G. Effective PID controller design using a novel hybrid algorithm for high order systems. *PLoS One*. **18**, e0286060. https://doi.org/10.1371/journal.pone.0286060 (2023).
4. Eker, E., Ekinci, S. & İzci, D. Optimal PID Controller Design for Liquid Level Tank via Modified Artificial Hummingbird Algorithm. *Comput. Sci. IDAP-2023*. 37–43. https://doi.org/10.53070/bbd.1346269 (2023).
5. Izci, D., Ekinci, S., Budak, C. & Gider, V. PID Controller Design for DFIG-based Wind Turbine via Reptile Search Algorithm, in: 2022 Global Energy Conference (GEC), IEEE, 2022: pp. 154–158. https://doi.org/10.1109/GEC55014.2022.9986617.
6. Raju, M., Saikia, L. C. & Sinha, N. Load frequency control of a multi-area system incorporating distributed generation resources, gate controlled series capacitor along with high-voltage direct current link using hybrid ALO-pattern search optimised fractional order controller. *IET Renew. Power Gener.* **13**, 330–341. https://doi.org/10.1049/iet-rpg.2018.5010 (2019).
7. Sahin, E. Design of an optimized fractional high order differential feedback controller for load frequency control of a multi-area multi-source power system with nonlinearity. *IEEE Access.* **8**, 12327–12342. https://doi.org/10.1109/ACCESS.2020.2966261 (2020).
8. Chehaibi, N. I., Ferfra, M., Rabeh, R. & Bouaddi, A. Optimizing Cascade-Loop Controller Parameters of Two-Area Autonomous Microgrid for Load Frequency Control Using Genetic Algorithm, in: 2024 International Conference on Control, Automation and Diagnosis (ICCAD), : pp. 1–6. (IEEE, 2024). https://doi.org/10.1109/ICCAD60883.2024.10553818
9. Sekyere, Y. O. M., Effah, F. B. & Okyere, P. Y. Optimally tuned cascaded FOPI-FOPIDN with improved PSO for load frequency control in interconnected power systems with RES. *J. Electr. Syst. Inform. Technol.* **11**, 25. https://doi.org/10.1186/s43067-024-00149-x (2024).

10. Masikana, S. B., Sharma, G., Sharma, S. & Çelik, E. Frequency regulation in solar PV-powered thermal power system using FPA-PID controller through UPFC and RFB. *Electr. Eng.*https://doi.org/10.1007/s00202-024-02417-5 (2024).
11. Shukla, H. et al. Implications of Energy Storage Device in Efficient Frequency Control of Multi-Area Power System, in: 2023 2nd International Conference on Clean Energy Storage and Power Engineering (CESPE), IEEE, : pp. 139–144. https://doi.org/10.1109/CESPE60923.2023.00035 (2023).
12. Kumar, A., Gupta, D. K., Ghatak, S. R., Novel Hybrid, A. & Optimized, I. G. S. A. B. P. S. O. FOPID Controller for load frequency control of multi-source Restructured Power System. *Recent. Adv. Electr. Electron. Eng. (Formerly Recent. Pat. Electr. Electron. Engineering)*. **16**, 726–749. https://doi.org/10.2174/2352096516666230427122716 (2023).
13. Ekinci, S. et al. Frequency regulation of PV-reheat thermal power system via a novel hybrid educational competition optimizer with pattern search and cascaded PDN-PI controller. *Results Eng.* 102958. (2024).
14. Jabari, M. et al. Efficient DC motor speed control using a novel multi-stage FOPD(1 + PI) controller optimized by the Pelican optimization algorithm. *Sci. Rep.* **14**, 22442. https://doi.org/10.1038/s41598-024-73409-5 (2024).
15. Pachauri, N. et al. A robust fractional-order control scheme for PV-penetrated grid-connected microgrid. *Mathematics* **11**(6), 1283 (2023).
16. Kalyan, C. H. et al. Squirrel search algorithm based intelligent controller for interconnected power system. *Int. J. Model. Simul.* 1–21 (2023).
17. Jena, N. et al. and. Impact of a redox flow battery on the frequency stability of a five-area system integrated with renewable sources energies. **16**(14), 5540. https://doi.org/10.3390/en16145540 (2023).
18. Benazeer Begum, N. K. et al. *Application of an Intelligent Fuzzy Logic Based Sliding mode Controller for Frequency Stability Analysis in a Deregulated Power System Using* (OPAL-RT platform Energy Reports, 2024).
19. Naga Sai, C. H. et al. Performance assessment of open loop and closed loop generation rate constraint models for optimal LFC of three area reheat thermal system. *Front. Energy Res.*https://doi.org/10.3389/fenrg.2022.920651 (2022).
20. Naga Sai, C. H. et al. Optimization Algorithm Based Fractional Order Fuzzy Controller for LFC of Multi Area Diverse Source System with realistic constraints. *Front. Energy Res.*https://doi.org/10.3389/fenrg.2022.921426 (2022).
21. Kalyan, C. H. N. S. et al. and. Water-cycle-algorithm-tuned Intelligent fuzzy controller for stability of multi-area multi-fuel power system with time delays. *Mathematics* **10**(3), 508. https://doi.org/10.3390/math10030508 (2022).
22. Kalyan, C. H., Siano, P., Kamel, S. Comparative Performance Assessment of Different Energy Storage Devices in Combined LFC and AVR Analysis of Multi-area Power System energies **15**(2), 629. https://doi.org/10.3390/en15020629 (2022).
23. Kalyan, C. N. S. et al. *Water Cycle Algorithm Optimized Type-II Fuzzy Controller for Load Frequency Control of Multi Area Multi Fuel System* (with Communication Time Delays, 2021).
24. Kalyan, C. N. S., Srikanth Goud, B., Reddy, C. R., Bajaj, M. & Srinivasa Rao, G. SMES and TCSC Coordinated Strategy for Multi-area Multi-source System with Water Cycle Algorithm Based 3DOF-PID Controller. *Smart Sci.*. https://doi.org/10.1080/23080477.2022.2054199 (2022).
25. Kalyan, C. N. et al. Soft Computing Algorithm-based Intelligent fuzzy Controller for enhancing the Network Stability of IPS. *Procedia Comput. Sci.* **235**, 3181–3190 (2024).
26. Kalyan, C. N. S., Gopi, P., Mohammadi, S. A. D. & Bajaj, M. Hybrid fuzzy PID control with HAEFA optimization for simultaneous voltage and frequency stabilization in multi-area diverse source power systems. *Cogent Eng.* **11** (1). https://doi.org/10.1080/23311916.2024.2391958 (2024).
27. Ram Babu, N. et al. A Comprehensive Review of recent strategies on Automatic Generation Control/Load frequency control in Power systems. *Arch. Comput. Methods Eng.* **30**, 543–572. https://doi.org/10.1007/s11831-022-09810-y (2023).
28. Guha, D., Roy, P. & Banerjee, S. Quasi-oppositional backtracking search algorithm to solve load frequency control Problem of Interconnected Power System. *Iran. J. Sci. Technol. Trans. Electr. Eng.* **44**, 781–804. https://doi.org/10.1007/s40998-019-00260-0 (2020).
29. Nowaková, J., Pokorný, M. & Pieš, M. Conventional controller design based on Takagi–Sugeno fuzzy models. *J. Appl. Log.* **13**, 148–155. https://doi.org/10.1016/j.jal.2014.11.008 (2015).
30. Nowaková, J. & Pokorný, M. Intelligent Controller Design by the Artificial Intelligence methods. *Sensors*. **20**, 4454. https://doi.org/10.3390/s20164454 (2020).
31. Eker, E. et al. Efficient voltage regulation: an RW-ARO optimized cascaded controller approach, E-Prime - advances in Electrical Engineering. *Electron. Energy*. **9**, 100687. https://doi.org/10.1016/j.prime.2024.100687 (2024).
32. Izci, D., Eker, E. & Ekinci, S. Parameter estimation of STM6-40/36 photovoltaic module using hybrid atom search particle swarm optimization. *Jordan J. Appl. Sci. - Nat. Sci. Ser.* **18**, 24–29. https://doi.org/10.35192/jjoas-n.v18i1.1825 (2024).
33. Izci, D., Ekinci, S. & Hussien, A. G. Efficient parameter extraction of photovoltaic models with a novel enhanced prairie dog optimization algorithm. *Sci. Rep.* **14**, 7945. https://doi.org/10.1038/s41598-024-58503-y (2024).
34. Ekinci, S., Izci, D. & Hussien, A. G. Comparative analysis of the hybrid gazelle-nelder–mead algorithm for parameter extraction and optimization of solar photovoltaic systems. *IET Renew. Power Gener.* **18**, 959–978. https://doi.org/10.1049/rpg2.12974 (2024).
35. Izci, D. & Ekinci, S. Fractional order controller design via gazelle optimizer for efficient speed regulation of micromotors, E-Prime -. *Adv. Electr. Eng. Electron. Energy*. **6**, 100295. https://doi.org/10.1016/j.prime.2023.100295 (2023).
36. Ekinci, S., Izci, D. & Yilmaz, M. Simulated annealing aided Artificial Hummingbird optimizer for infinite impulse response system identification. *IEEE Access*. **11**, 88627–88636. https://doi.org/10.1109/ACCESS.2023.3303328 (2023).
37. Gupta, D. K. et al. Load Frequency Control Using Hybrid Intelligent Optimization Technique for Multi-Source Power Systems, *Energies (Basel)* **14** 1581. https://doi.org/10.3390/en14061581. (2021).
38. Ibrahim, M. H., Ang, S. P., Hamid, Z., Mohammed, S. S. & Law, K. H. A Comparative Hybrid Optimisation Analysis of Load Frequency Control in a Single Area Power System Using Metaheuristic Algorithms and Linear Quadratic Regulator, in: 2022 International Conference on Green Energy, Computing and Sustainable Technology (GECOST), IEEE, : pp. 232–237. (2022). https://doi.org/10.1109/GECOST55694.2022.10010488
39. Mahboob Ul Hassan, S., Ramli, M. A. M. & Milyani, A. H. Robust load frequency control of Hybrid Solar Power systems using optimization techniques. *Front. Energy Res.* **10**. https://doi.org/10.3389/fenrg.2022.902776 (2022).
40. Ramjug-Ballgobin, R. & Ramlukon, C. A hybrid metaheuristic optimisation technique for load frequency control. *SN Appl. Sci.* **3**, 547. https://doi.org/10.1007/s42452-021-04482-y (2021).
41. Kayri, M., Ipek, C., Izci, D. & Eker, E. A Novel Hybrid Metaheuristic Algorithm and its comparative performance Assessment. *Electrica*. **22**, 143–159. https://doi.org/10.54614/electrica.2022.21112 (2022).
42. Izci, D., Ekinci, S., Novel Hybrid, A. & Algorithm, A. S. O. N. M. and Its Application to Automobile Cruise Control System, in: G. Mathur, M. Bundele, L. Mahendra, M. Paprzycki (Eds.), 2nd International Conference on Artificial Intelligence: Advances and Applications, 1st ed., Springer Singapore, : pp. 333–343. https://doi.org/10.1007/978-981-16-6332-1_29 (2022).
43. Izci, D., Ekinci, S. & Hekimoğlu, B. Fractional-order PID Controller Design for Buck Converter System via Hybrid Lévy Flight distribution and simulated annealing algorithm. *Arab. J. Sci. Eng.* **47**, 13729–13747. https://doi.org/10.1007/s13369-021-06383-z (2022).
44. Eker, E., Kayri, M., Ekinci, S. & Izci, D. A New Fusion of ASO with SA Algorithm and its applications to MLP Training and DC Motor Speed Control. *Arab. J. Sci. Eng.* **46**, 3889–3911. https://doi.org/10.1007/s13369-020-05228-5 (2021).
45. Zhao, W. et al. Quadratic interpolation optimization (QIO): a new optimization algorithm based on generalized quadratic interpolation and its applications to real-world engineering problems. *Comput. Methods Appl. Mech. Eng.* **417**, 116446. https://doi.org/10.1016/j.cma.2023.116446 (2023).

46. Abualigah, L., Izci, D., Ekinci, S., Zitar, R. A. & Controller Optimizing Aircraft Pitch Control Systems: A Novel Approach Integrating Artificial Rabbits Optimizer with PID-F *Int. J. Rob. Control Syst.* **4** 354–364. https://doi.org/10.31763/ijrcs.v4i1.1347. (2024).
47. Izci, D., Ekinci, S., Eker, E. & Demirören, A. Multi-strategy modified INFO algorithm: performance analysis and application to functional electrical stimulation system. *J. Comput. Sci.* **64**, 101836. https://doi.org/10.1016/j.jocs.2022.101836 (2022).
48. Kirkpatrick, S., Gelatt, C. D. & Vecchi, M. P. Optimization by simulated annealing. *Science.* **220** (1983), 671–680. https://doi.org/10.1126/science.220.4598.671 (1979).
49. Abualigah, L., Ekinci, S. & Izci, D. Aircraft Pitch Control via filtered proportional-integral-derivative Controller Design using Sinh Cosh Optimizer. *Int. J. Rob. Control Syst.* **4**, 746–757. https://doi.org/10.31763/ijrcs.v4i2.1433 (2024).
50. Ekinci, S. et al. Automatic Generation Control of a hybrid PV-Reheat Thermal Power System using RIME algorithm. *IEEE Access.* **12**, 26919–26930. https://doi.org/10.1109/ACCESS.2024.3367011 (2024).
51. Khadanga, R. K., Kumar, A. & Panda, S. A novel modified whale optimization algorithm for load frequency controller design of a two-area power system composing of PV grid and thermal generator. *Neural Comput. Appl.* **32**, 8205–8216. https://doi.org/10.1007/s00521-019-04321-7 (2020).
52. Abd-Elazim, S. M. & Ali, E. S. Load frequency controller design of a two-area system composing of PV grid and thermal generator via firefly algorithm. *Neural Comput. Appl.* **30**, 607–616. https://doi.org/10.1007/s00521-016-2668-y (2018).
53. Çelik, E., Öztürk, N. & Houssein, E. H. Influence of energy storage device on load frequency control of an interconnected dual-area thermal and solar photovoltaic power system. *Neural Comput. Appl.* **34**, 20083–20099. https://doi.org/10.1007/s00521-022-07558-x (2022).
54. Can, O. & Ayas, M. S. Gorilla troops optimization-based load frequency control in PV-thermal power system. *Neural Comput. Appl.* **36**, 4179–4193. https://doi.org/10.1007/s00521-023-09273-7 (2024).
55. Izci, D. Design and application of an optimally tuned PID controller for DC motor speed regulation via a novel hybrid Lévy flight distribution and nelder–mead algorithm. *Trans. Inst. Meas. Control.* **43**, 3195–3211. https://doi.org/10.1177/01423312211019633 (2021).
56. Izci, D., Ekinci, S. & Hussien, A. G. An elite approach to re-design Aquila optimizer for efficient AFR system control. *PLoS One.* **18**, e0291788. https://doi.org/10.1371/journal.pone.0291788 (2023).


## Acknowledgements

This article has been produced with the financial support of the European Union under the REFRESH – Research Excellence For Region Sustainability and High-tech Industries project number CZ.10.03.01/00/22_003/0000048 via the Operational Programme Just Transition and paper was supported by the following project TN02000025 National Centre for Energy II.

## Author contributions

Davut Izci, Serdar Ekinci: Conceptualization, Methodology, Software, Visualization, Investigation, Writing-Original draft preparation. Emre Çelik: Data curation, Validation, Supervision, Resources, Writing - Review & Editing. Mohit Bajaj, Lukas Prokop, Vojtech Blazek: Project administration, Supervision, Resources, Writing - Review & Editing.

## Declarations

## Competing interests

The authors declare no competing interests.

## Additional information

**Correspondence** and requests for materials should be addressed to M.B.

**Reprints and permissions information** is available at www.nature.com/reprints.

**Publisher's note** Springer Nature remains neutral with regard to jurisdictional claims in published maps and institutional affiliations.